Corrosion Science 183 (2021) 109345

Contents lists available at ScienceDirect

Corrosion Science

journal homepage: www.elsevier.com/locate/corsci

Laser ablation behavior of C/SiC composites subjected to transverse hypersonic airflow

Zhe Wang [a,b], Jiangtao Wang [a,b], Hongwei Song [a,b,*], Wu Yuan [a,b], Yuwen Liu [c], Te Ma [a,b], Chenguang Huang [b]

[a] Key Laboratory for Mechanics in Fluid-Solid Coupling Systems, Institute of Mechanics, Chinese Academy of Sciences, Beijing, 100190, China
[b] School of Engineering Sciences, University of Chinese Academy of Sciences, Beijing, 100049, China
[c] School of Environmental and Chemical Engineering, Yanshan University, Qinhuangdao, Hebei, 066004, China

ARTICLE INFO

Keywords:
Laser ablation (C)
C/SiC composite (A)
Hypersonic airflow (C)
Ablation morphology (C)
Mechanical erosion (C)

ABSTRACT

Laser ablation behaviors of C/SiC composites were examined in a hypersonic wind tunnel. Parallel laser ablation tests under static air were also conducted, and the ablation behaviors of these two conditions were compared. Mass ablation rates were augmented by 4–9 times when subjected to the hypersonic airflow. Ablation morphologies were significantly different in the micro and macro scales, and the needle-like microstructure of carbon fibers under static air turned to be rough and tattered under the hypersonic airflow. The accelerated ablation rate and the peculiar ablation micro-morphologies were mainly attributed to the strong mechanical erosion induced by hypersonic airflow.

1. Introduction

Continuous fiber-reinforced ceramic matrix composites (CMCs) are attracting considerable interest and increasingly applied in aerospace fields due to their high specific stiffness and strength, high temperature tolerance, and good thermal shock resistance [1–4]. As one of the most topical CMCs, C/SiC composites are promising materials for thermal protection systems (TPS) in the development of hypersonic flights. The ablation performance of the C/SiC composite is closely related to its practical service life and has a remarkable effect on the optimal design of hypersonic vehicle structures [5–8].

Conventional experimental methods for the ablation test of C/SiC composites are the oxyacetylene flame and the plasma arc [9–14], and the examination of the morphology and the microstructure of C/SiC composite after ablation is a typical method to learn ablation mechanisms [13,14]. Generally, the ablation morphology can be divided into three regions, i.e., center, transition, and edge regions [9,13]. Chen [14] has compared the morphology and the microstructure of the ablation center of C/SiC by using the oxy-acetylene flame at different temperatures. The sublimation of the carbon fiber and SiC matrix are the main ablation behavior above 3550 °C, and the thermal decomposition and the oxidation of the SiC matrix are the main ablation behaviors at 2900 °C. Typically, C/SiC composites are used in high-enthalpy and high-speed airflow environments, thereby facing the conditions of high temperature, high pressure, and strong erosion. Some researchers have used the arc and the plasma wind tunnels to study the ablation characteristics of C/SiC composites for the simulation of the service environment of high-speed and high-enthalpy chemical nonequilibrium airflow [15–17]. The incoming flow affects the oxidation rate and accelerates the ablation process due to the erosion effect [16].

Some researchers have studied the ablation morphology of composites at the multiscale level [18–21]. For C/C composites, the micro ablation morphologies of carbon fiber and matrix are affected by two competitive regimes of reaction-limited and diffusion-limited [20]. Carbon fibers have a needled shape under fast diffusion and ogival shapes under fast reaction. Similar phenomena also appear in C/SiC composites [13,14]. Micro morphologies are closely related to ablation conditions and affect the ablation behavior under high-speed airflow conditions [21].

Given the advantages of the stable ablation energy and the non-additional chemical reaction, the high-energy laser has become a new method to study the ablation behavior. And the laser ablation performance of thermal protection materials has become a research focus [22–27]. Research shows that the sublimation and the physical erosion

* Corresponding author at: Key Laboratory for Mechanics in Fluid-Solid Coupling Systems, Institute of Mechanics, Chinese Academy of Sciences, Beijing, 100190, China.
E-mail address: songhw@imech.ac.cn (H. Song).

https://doi.org/10.1016/j.corsci.2021.109345
Received 24 November 2020; Received in revised form 22 February 2021; Accepted 23 February 2021
Available online 25 February 2021
0010-938X/

are the main causes of the evolution of the ablation center due to the local low oxygen and the high heat flux environment induced by the high-energy laser [26]. Wang [27] has investigated the effect of the transverse supersonic airflow on the laser ablation of C/SiC composites experimentally. The laser ablation rates of C/SiC composites were augmented by the supersonic airflow. Moreover, the ablation morphologies and the microstructure of C/SiC composites are quite different from those in the static air environment.

Aerodynamic force and heat in hypersonic conditions are more severe compared with those in static and supersonic environments. And in some situations, the material surface is subjected to the vertically high heat flux together with the transverse hypersonic airflow, bringing more complex mechanisms on the ablation progress. Thus, the effects of transverse hypersonic airflow on the laser ablation behavior of C/SiC composites, which is different from that of conventional conditions, are also worthy of study. This research is helpful to estimate the service limit and the ablation endurance of C/SiC in some extreme conditions. However, reports on the ablation behaviors of C/SiC composites caused by the coupling effect of the high local heat flux induced by intense laser and high-enthalpy hypersonic airflow remain unavailable. In the present study, a continuous wave laser beam is used as heat source to investigate the ablation resistance of C/SiC composites in a hypersonic wind tunnel. Parallel laser ablation tests are also performed in a static air environment. The experimental results of the two conditions are compared, and the morphologies, microstructure, and mechanisms of laser ablation behaviors of C/SiC composites subjected to the transverse hypersonic airflow are elucidated. Ablation models are introduced to evaluate the contribution of the accelerated ablation due to different mechanisms.

2. Experimental

2.1. Materials

C/SiC composites with two different carbon fiber preforms, i.e., two-dimensional woven (2D) and three-dimensional needle (3DN), were tested. C/SiC samples were fabricated via the chemical vapor infiltration (CVI) process by the Science and Technology on Thermostructural Composite Materials Laboratory, Northwestern Polytechnical University, PR China. The 2D preform was made of stacking plain weave carbon cloths (PAN, T-300, Toray Co., Japan) [28]. The 3DN preform was composed of orthogonal non-woven carbon cloths (0°, 90°) and the short cut net ply that repeatedly superimposed for desired thickness. The needling process was carried out to keep adjacent units together with carbon fibers [29]. Carbon fiber preforms were densified by the depositing the pyrocarbon (PyC) interphase with a thickness of 200 nm, and then the preforms were heat-treated at 1800 °C for 2 h under vacuum. Porous preforms were fabricated through the deposition of the SiC matrix via the low-pressure CVI process: the deposition temperature was 1000 °C, pressure was 5 kPa, time was 240 h, the molar ratio of H_2 to MTS (CH_3SiCl_3) was 10 [26,30]. The 2D and the 3DN C/SiC composites were prepared using this method. Moreover, Ti_3SiC_2-modified 2D C/SiC composites were fabricated through slurry and liquid silicon infiltration (LSI) methods. The introduction of the Ti_3SiC_2 matrix decreases the ablation rate of composites [30]. The properties of C/SiC composites tested in the present study are shown in Table 1.

Table 1
The properties of different C/SiC composites.

Composites	Density (g/cm^3)	Porosity (vol%)	Bending strength (MPa)	Bending modulus (GPa)	Fracture toughness ($MPa{\cdot}m^{1/2}$)
2D C/SiC	2.00	13	539 ± 39	–	22.3 ± 1.0
2D C/SiC-Ti_3SiC_2	2.42	8	447 ± 25	42 ± 2	16.1 ± 1.1
3DN C/SiC	2.10	18	242 ± 38	46 ± 10	18 ± 7.0

2.2. Laser ablation setup

A continuous wave laser device was used in the ablation test (YLS-2000 IPG fiber laser). The laser beam was irradiated on the center of the C/SiC sample with a vertical angle of 90°. The size of samples for ablation tests was 50 mm × 50 mm × 2 mm. Table 2 shows the main parameters of the laser device in the ablation test.

2.3. Experimental environment setup

As shown in Fig. 1, the laser ablation tests of C/SiC composites were conducted in a hypersonic free jet wind tunnel with the freestream of Mach 6.0. High-enthalpy and high-pressure gases produced by hydrogen-oxygen combustion were conveyed as high-speed airflow in the hypersonic wind tunnel [31]. The C/SiC composite was installed on a specially designed fixture inside the wind tunnel. The laser beam was delivered to the C/SiC sample through the airtight observation window. The instantaneous response of the sample on the back surface was acquired with measurement devices through the observation window on the other side. The temperature of the back surface was measured by colorimetric temperature measurement (Fluke Endurance). Furthermore, the laser and the measuring equipment were synchronously triggered and controlled by the wind tunnel system. Some parameters of the freestream in the ablation test are shown in Table 3. Comparative tests under static air were also conducted at the same test parameters.

2.4. Characterization

The microstructure of ablated composites and the composition of ablation products were captured using scanning electron microscopy and energy-dispersive spectrometry (SEM and EDS, respectively; Hitachi-S3400). The depth and the 3D morphologies of ablation pits were measured using the Bruker DektakXT profiling system and the HIROX KH-8700 3D digital microscope system, respectively. The mass loss of the laser-ablated samples was determined using a laboratory balance (±0.1 mg). The mass ablation rate (R_m, mg/s) of the ablated sample was calculated in accordance with the formula:

$$R_m = \frac{m_0 - m_t}{t}, \tag{1}$$

where m_0 and m_t are the sample weights before and after ablation (mg), respectively, and t is the ablation time (s).

3. Results and discussion

3.1. Aerodynamic cooling effect of airflows

Fig. 2 shows back-surface temperature histories in two environments. The back-surface temperature of C/SiC before laser irradiation was approximately 640 K (period 1 in Fig. 2) due to the aerodynamic heating. Upon laser irradiation, the back-surface temperature in the hypersonic airflow environment was lower than that in the static air environment due to aerodynamic cooling effects. According to Newton's law of cooling,

Table 2
Main parameters of the laser device in the ablation test.

Parameters	Value
Laser wavelength (nm)	1070
Laser power (W)	2000
Spot diameter (mm)	10
Laser power density(W/cm^2)	2546
Irradiation time (s)	4
Ambient temperature (K)	293

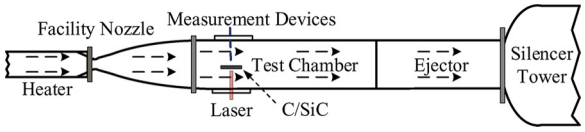

Fig. 1. Schematic of the laser ablation tests system in the hypersonic wind tunnel.

Table 3
The parameters of the freestream in the ablation test.

Parameters	Value
Total temperature (K)	1784
Static temperature (K)	222.4
Total pressure (kPa)	4257
Static pressure (kPa)	2.550
Mach number	6.0

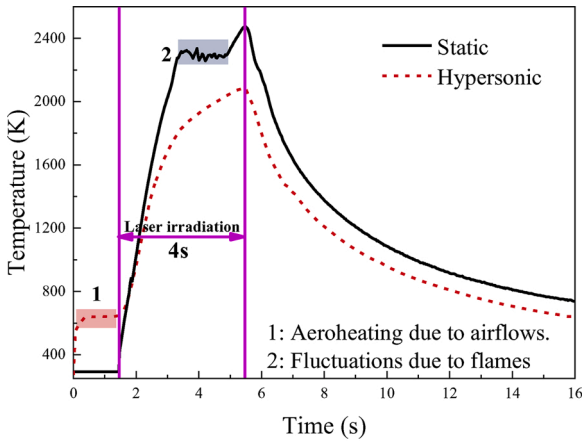

(a)

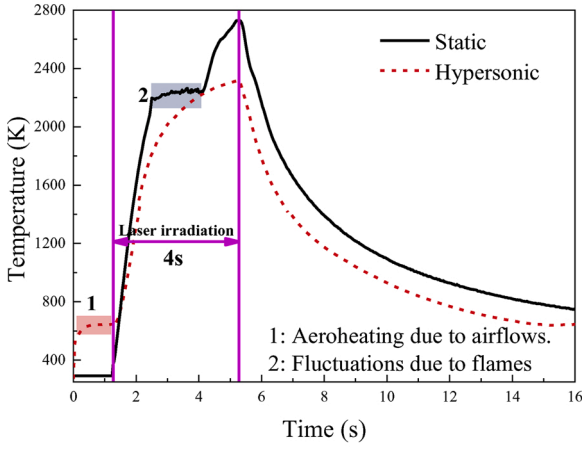

(b)

Fig. 2. Back-surface temperature of C/SiC sample in the two environments: (a) 2D C/SiC, (b) 3DN C/SiC.

$$-\lambda \left.\frac{\partial T}{\partial x}\right|_{x=0} = h\left[T_f - T_w(x,t)\right], \tag{2}$$

where λ is the thermal conductivity (W/m·K), h is the surface heat transfer coefficient due to airflow properties and velocity (W/m^2·K), T_f is the ambient airflow temperature (K), and T_w is the wall temperature of the heating surface (surface temperature of samples, K).

The sublimation temperature of C/SiC sample was beyond 3000 K, and upon laser irradiation, T_w was soon higher than 2000 K. By contrast, the static temperature and the total temperature of Ma 6.0 airflow were below 250 K and 1800 K, respectively, in the present test. It indicated that T_f was much lower than T_w and the airflow was taking away heat from the ablation surface continuously. Also, the surface heat transfer coefficient (h) increased as the airflow speed increased. Thus, compared with static air, the hypersonic airflow had significant cooling effects on the laser irradiation surface during the ablation stage.

The thermal response time of the 3DN C/SiC sample was faster than that of the 2D C/SiC sample (Fig. 2a and b), because the low thermal conductivity of matrix and the weak interlayer bonding of 2D C/SiC led to slow heat transfer in the interlaminar direction. By contrast, the high thermal conductivity of the carbon fiber and the structural integrity of 3DN C/SiC maintained high through-thickness heat transfer. Therefore, 2D C/SiC had lower thermal diffusivity than 3DN in the thickness direction.

3.2. Macroscopic morphologies and ablation rates

Fig. 3 shows the laser ablation morphologies of the ablated 2D and 3DN C/SiC samples reconstructed by the 3D digital microscope system. Despite the cooling effect of airflow, the ablation damage of C/SiC composites subjected to the hypersonic airflow was exacerbated remarkably. The maximum ablation depth in the hypersonic airflow environment was greater than that in the static air environment, and the surface of ablation pits was also smoother. Three ablation regions with well-defined boundaries were clearly distinguished in static results, and these results were similar to those reported in the previous work [25]. By comparison, the boundaries of the three regions in the hypersonic results were blurred. The area of the white oxide layer visibly decreased. Moreover, the aerodynamic erosion effects, which made the ablation pit asymmetric, were evident downstream of the ablation pits under airflow.

The depth of ablation pits was analyzed further through the profiling system. Fig. 4 shows the comparison of the profile of ablation pits along the central axis of the 2D and 3DN C/SiC samples in the two environments. Ablation pits under hypersonic airflow were larger and deeper compared with those in the static environment. For 2D C/SiC composites, the maximum depths in the static and the hypersonic results were 801 and 1216 μm, respectively. Moreover, the depths of the 3DN C/SiC in the static and the hypersonic environments increased to 1145 and over 1270 μm, respectively. A fast temperature transfer in the thickness direction occurred in 3DN samples (Section. 3.1), resulting in a large ablation depth under both airflow conditions. Profiling results regularly accorded with the results of the 3D digital microscope system in Fig. 3. Aerodynamic erosion effects accelerated the removal of the ablation boundary and resulted in a relatively smooth ablation surface in the hypersonic environment.

Fig. 5 shows the mass ablation rates (R_m) of C/SiC composites. The average mass ablation rates of 2D, 3DN, and 2D Ti_3SiC_2-modified samples were 22.8, 29.3, and 13.2 mg/s, respectively, under static air; and increased to 116.8, 142.2, and 131.7 mg/s, respectively, under hypersonic airflow. The ablation rates of 2D and 3DN samples in the hypersonic environment were approximately augmented by 4 times compared to those in the static air. The reason for increased ablation rates will be discussed in the next sections. Among the three kinds of materials, 3DN C/SiC composites had the highest porosities because of their specific structural design and knitting process. High porosity and insufficient

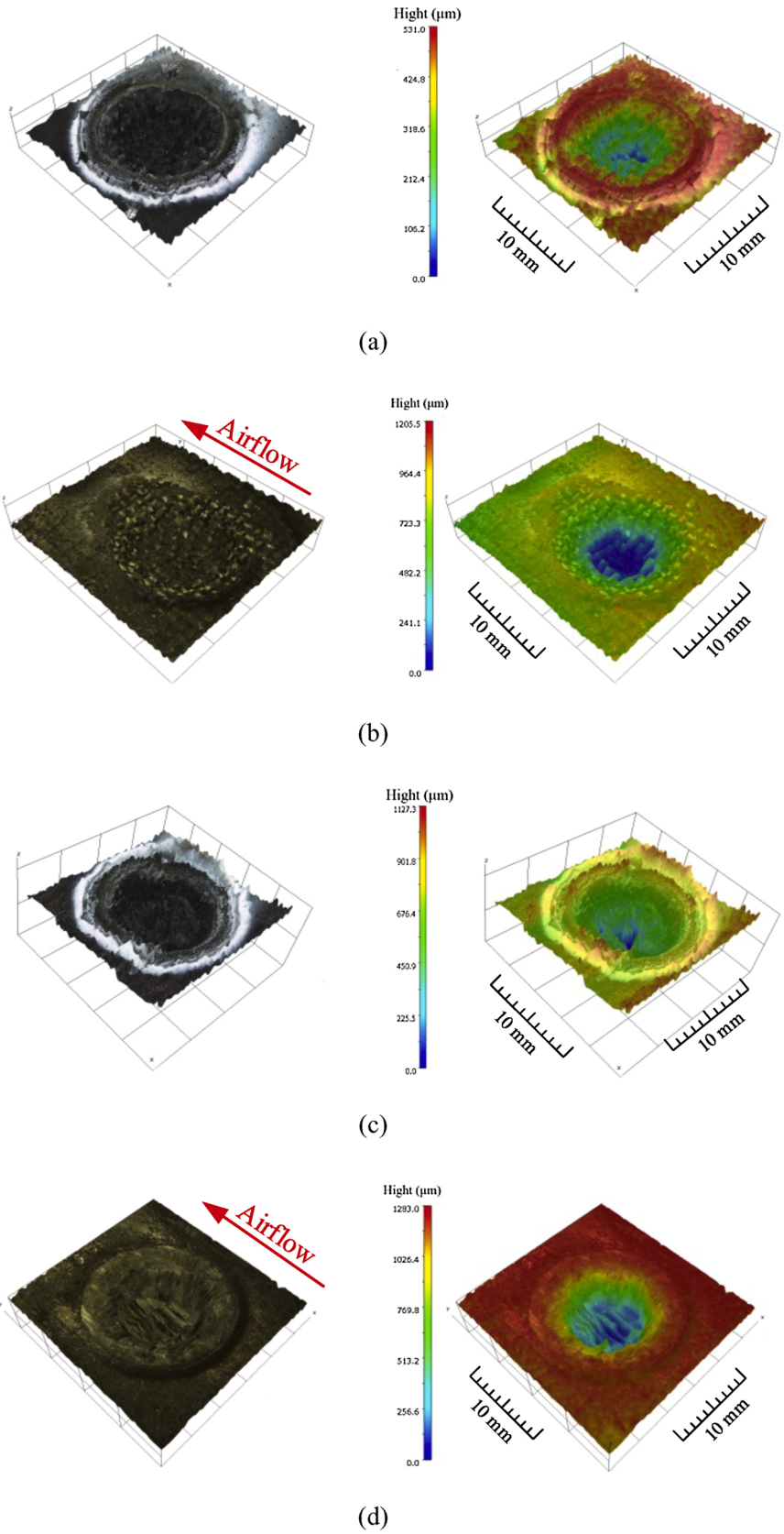

Fig. 3. 3D morphologies of ablated C/SiC in different environments: (a) 2D C/SiC in the static air environment; (b) 2D C/SiC in the hypersonic airflow environment, (c) 3DN C/SiC in the static air environment, (d) 3DN C/SiC in the hypersonic airflow environment.

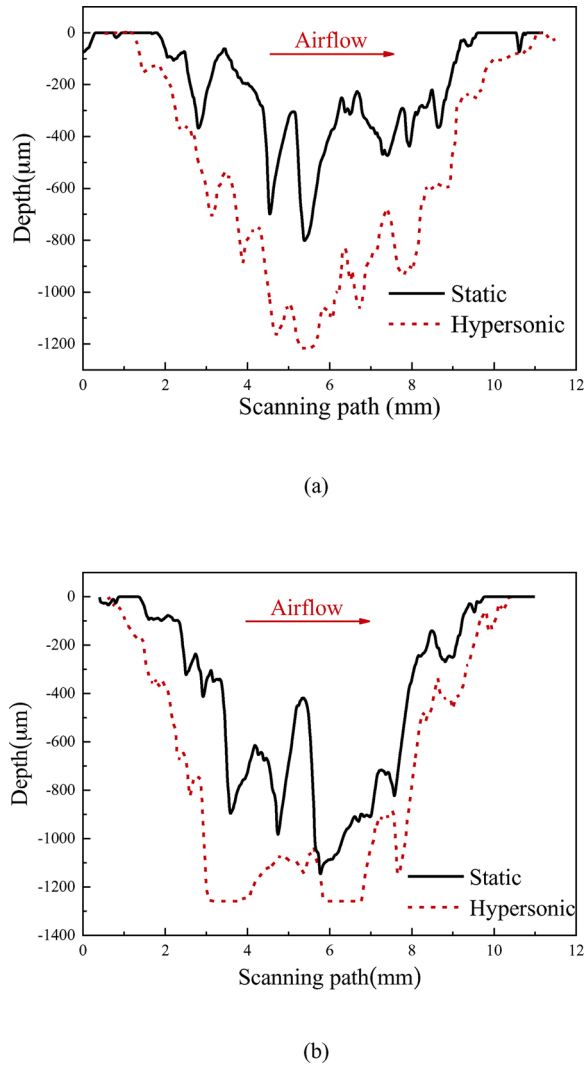

Fig. 4. Profile of ablation pits along the central axis in the two environments: (a) 2D C/SiC, (b) 3DN C/SiC.

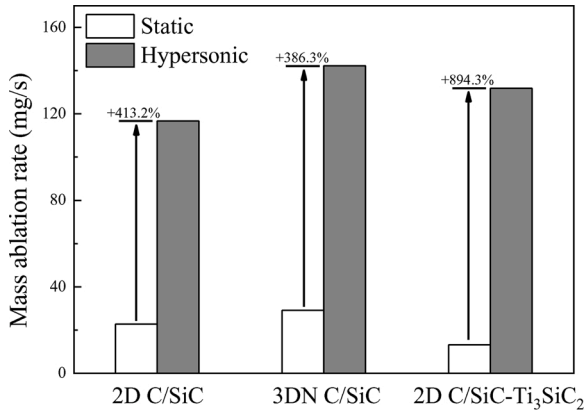

Fig. 5. Mass ablation rate of C/SiC composites in the two environments.

compactness resulted in great oxygen diffusion and oxidation reaction rates. Moreover, the 3DN sample had higher thermal diffusivity than the 2D sample in the thickness direction. Under high heat flux conditions, the temperature of the surface rapidly reached the ablation temperature, and the higher thermal diffusion ability in the thickness, the faster the ablation front develops. Thus, a deeper ablation depth and more mass loss occurred in 3DN samples. Therefore, the ablation mass loss of the 3DN C/SiC was both the highest under the static air and airflow conditions. The experimental results of the Ti_3SiC_2-modified C/SiC under static air showed that the modification method was effective in the ablation resistance, and this finding agreed with that in previous work [30]. However, in the hypersonic airflow environment, the ablation rates 2D-modified sample were augmented by 9 times compared to it in the static air. The laser ablation resistance of the 2D-modified sample was lower than that of the 2D-unmodified sample. The oxides existing on the ablation surface of C/SiC–Ti_3SiC_2 were mainly composed of SiO_2 and TiO_2 [30], and the melting points of SiO_2 and TiO_2 were about 1720 °C and 1840 °C, respectively. The oxides were in liquid form and exhibited little strength at high temperatures in the ablation region. Thus, the oxides were easily blown away when subjected to high-speed airflow. However, the densities of TiO_2 and SiO_2 are 4.2 g/cm^3 and 2.2 g/cm^3, respectively. The addition of Ti_3SiC_2 to C/SiC increases the total mass fraction of liquified oxidation products at high temperatures, i.e., the mass fraction of liquids generated in C/SiC–Ti_3SiC_2 (TiO_2 and SiO_2) was higher than that generated in the C/SiC sample (only SiO_2). Thus, the Ti_3SiC_2-modified sample had more mass loss than the unmodified sample. Therefore, the difference was partly because of the mechanical erosion of the extra titanium compounds induced by the aerodynamic force at high temperatures.

3.3. Microscopic morphologies and microstructure

Fig. 6 (a)–(b) show SEM and EDS results for the ablation pits of the 2D C/SiC composites in the two environments. Regions A–C (or D-F) were the center, transition, and edge regions of the ablation pit, respectively. Areas 1–4 were marked, and the component analysis was given. In the static air environment, the carbon fibers at the center region exhibited a needle-like structure (Fig. 6a). At the ablation transitional region, the SiC particles with an atomic proportion of silicon and carbon of 54.67:45.33 were identified clearly in Area 1. The white layer with an atomic proportion of silicon and oxygen of 37.11:62.89 in Area 2 was the solidification of silicon oxides at the edge region.

The microscopic ablation morphologies of C/SiC composites in the hypersonic airflow environment are given in Fig. 6(b). Intense ablation damage and aerodynamic erosion effects appeared at the ablation center region of the ablation pit. Carbon fibers were torn and roughened by the hypersonic airflow. The SiC particles that formed at the transition region of the samples in the static air environment almost vanished due to the erosion effect. Area 3 was composed of silicon, carbon, and oxygen with a ratio of 34.11:51.79:14.10 following the EDS results. The component analysis illustrated that residual fibers and the partially oxidized SiC matrix remained at the ablation transition region. Compared with those in the static environment, the silicon oxide layer with an approximate ratio of 34.75:65.25 for silicon and oxygen were deposited and partially exfoliated in the downstream area of the hypersonic airflow environment.

As shown in Fig. 7(a), carbon fibers with the needle-like structure were seen in the ablation center of the C/SiC sample in the static air environment. The morphologies were mainly due to the difference in the ablation reactivity between the matrix and the fiber. The SiC matrix was more ablated than the carbon fiber under high temperature, and carbon fibers were exposed to air. The needle-like structure was a result of the competition between diffusion and reaction of exposed carbon fiber, which was elaborated in previous work [20]. By contrast, the fibers exhibited an evident rough and tattered morphology in Fig. 7(b). When air was flowing on the ablation surface, the diffusion of oxidation gas inside the material was accelerated. The ablation regime was more reaction-limited in the ablation center, and the difference in the reactivity between the matrix and the fiber was increased. Thus, the fiber was exposed for a longer length. Furthermore, this difference in the microscopic structures was due to the heterogeneities of the carbon structure inside carbon fibers, and the impact by high-speed airflow and

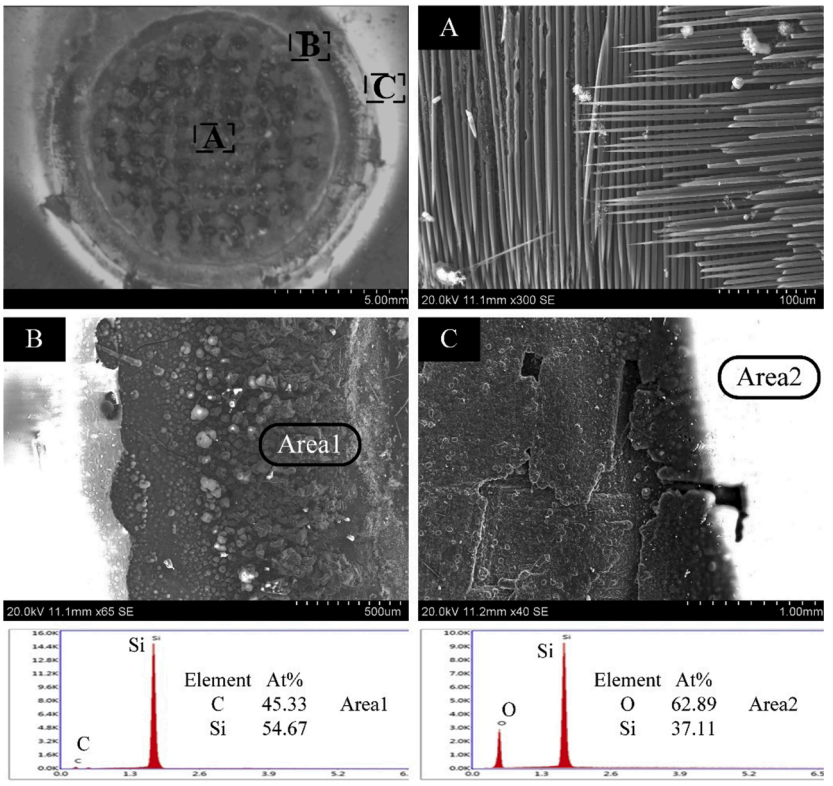

(a)

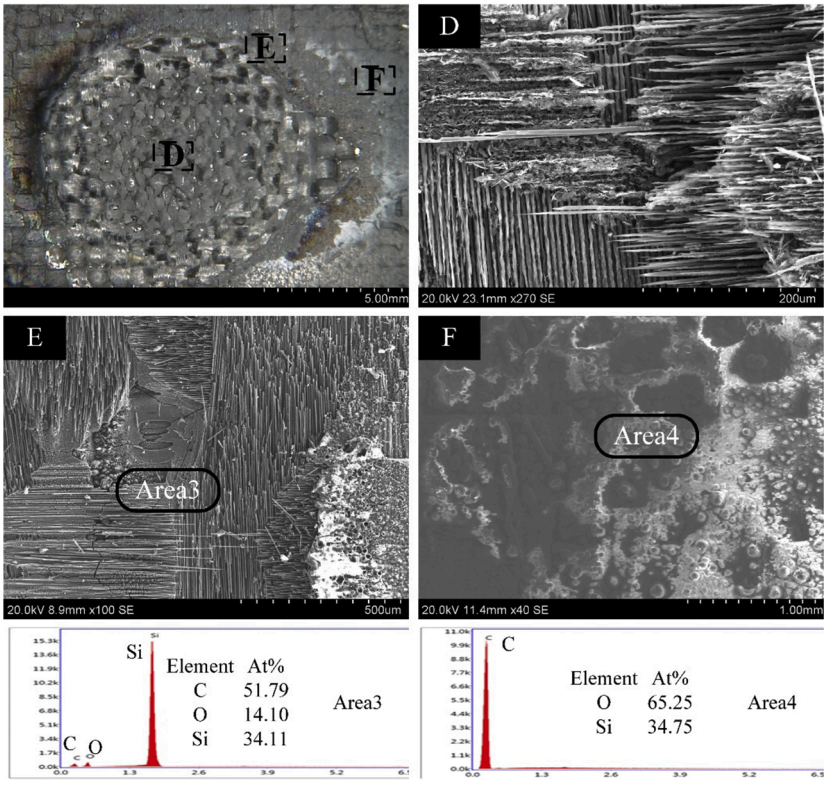

(b)

Fig. 6. SEM and EDS results for the ablation pits of the 2D C/SiC composites in the two environments: (a) Static, (b) Hypersonic.

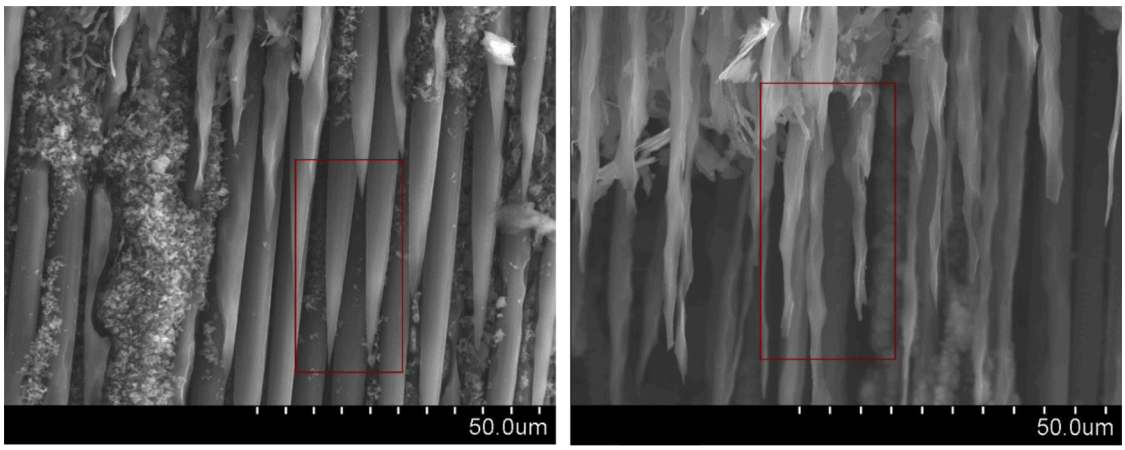

Fig. 7. Microscopic morphologies of the ablated carbon fibers in the two environments: (a) Static, (b) Hypersonic.

the particles of ablation products at high temperatures. The phenomenon illustrated that ablation morphologies were also significantly different at the micro-scale, and intense effects of aerodynamic erosion were both reflected macroscopically and microscopically.

3.4. Ablation mechanisms

The temperature difference between the ablation surface and back surfaces can be estimated in accordance with the Fourier's Law:

$$q = -\lambda \frac{\partial T}{\partial n} \approx \lambda \frac{\Delta T}{\Delta z}, \tag{3}$$

where ΔT is the temperature difference between the front surface and the back surface, Δz is the thickness of specimen, λ is the thermal conductivity in thickness direction, $\partial T/\partial n$ is the temperature gradient in the n-direction (thickness direction), and q is the heat flux density input to the ablation surface.

Considering the laser energy, radiation, convection, and reaction heat on the ablation surface, and thickness changing of samples at the ablation center, q, λ, and Δz take the value of 1.2×10^7 W/m^2, 10/14 (2D/3DN) W/m·K [28], and 1.5–2 $\times$ 10^{-3} m, respectively. Therefore, ΔT was evaluated at about 1800–2400/1286–1714 K for 2D/3DN C/SiC composites. The sublimation temperatures of carbon fibers and the SiC matrix were above 3600 and approximately 3000 K, respectively. Thus, the temperature of the ablation center was assumed to be above the sublimation temperature of carbon fibers.

The laser ablation mechanisms of the three regions under static air were different. The SiC matrix was more ablated than the carbon fiber. Thus, the sublimation of the SiC matrix was adequate, and partially sublimed carbon fibers were exposed to air. Moreover, the decomposition of the partial SiC matrix and the oxidation reaction of residual carbon fiber were also involved. Thus, the needle-like structure of fiber was due to the difference in the ablation reactivity between the matrix and the fiber, and the competition between diffusion and reaction of the fiber. The temperature of the ablation transition region was lower than that of the ablation center. It was insufficient to induce the sublimation and decomposition of SiC matrix. Thus, the ablation was dominated by the partial oxidation of the carbon fibers and the SiC matrix, and SiC particles were protuberant on the ablation surface. At the ablation edge region, the liquid silicon oxide solidified and was deposited as a result of relatively low temperature, thereby preventing the further oxidization of material in this region.

The laser ablation mechanisms of the three regions changed due to the hypersonic airflow. Tattered structures instead of needle-like were found for ablated carbon fibers in the center region, due to the heterogeneities of carbon structure and the impact by high-speed airflow and solid ablation products. In the transition region, SiC particles were blown away, residual fibers and the partially oxidized matrix remained. In the edge region, when the air was flowing over, silicon oxide exhibited low strength and was massively exfoliated owing to the influence of aerodynamic forces. Therefore, the oxidation reaction was aggravated. On the basis of the analysis above, the reactions were as follows [14]:

$$C(s) = C(g), \tag{4}$$

$$SiC(s) = SiC(g), \tag{5}$$

$$SiC(s) = Si(g) + C(g), \tag{6}$$

$$2SiC(s) + 3O_2(g) = 2SiO_2(l) + 2CO(g), \tag{7}$$

$$SiC(s) + O_2(g) = SiO(g) + CO(g), \tag{8}$$

$$Si(s) + O_2(g) = SiO_2(l), \tag{9}$$

$$SiO_2(l) + CO(g) = SiO(g) + CO_2(g), \tag{10}$$

$$2C(g) + O_2(g) = 2CO(g), \tag{11}$$

$$C(g) + O_2(g) = CO_2(g). \tag{12}$$

When the hypersonic air was flowing over the ablation surface, the diffusion of oxidation gas on the ablation surface was accelerated. The oxygen transferred to the ablation surface was sufficient for the oxidation reaction. Thus, the oxidation reaction was reaction-limited instead of diffusion-limited. Thus, the fiber was exposed for a longer length in the ablation center, and the oxidation reaction increased in the transition region. In addition, massive ablation products (i.e., SiC particles and liquid SiO_2) were removed, and the oxidation reaction was aggravated in the edge region. Therefore, the oxidation reaction increased under airflow, and mass ablation rates (R_m) significantly accelerated. The laser ablation behaviors of the C/SiC composites subjected to the hypersonic airflow were the combined effects of sublimation, increased oxidation, and intense aerodynamic erosion. Despite the cooling effect that occurred on the ablation surface, the aerodynamic erosion induced by hypersonic airflow accelerated the laser ablation.

3.5. Ablation models

As shown in Fig. 8, the energy conservation on the ablation surface is:

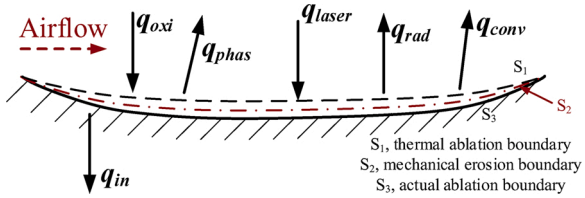

Fig. 8. The energy conservation on ablation surface of C/SiC composite.

$$q_{in} = -\lambda\frac{\partial T}{\partial n} = \alpha q_{laser} - q_{rad} - q_{conv} - q_{phas} + q_{oxi}, \tag{13}$$

where λ is the thermal conductivity in the thickness direction, $\partial T/\partial n$ is the temperature gradient in the n-direction (thickness direction), q_{laser} is the incident laser energy density, α is the laser energy coupling coefficient, q_{rad} is the heat flux radiated from the ablation boundary to the ambient airflow, q_{conv} is the convective heat transfer between the ablation boundary and the ambient airflow, q_{oxi} is the heat flow released by the oxidation reaction, q_{phas} is the heat flux consumed by the sublimation reaction, and q_{in} is the heat flux density transferred into the material.

In addition, mass conservation is followed on the ablation surface.

$$\dot{m}_{w-i} = \dot{m}_{iw} - \dot{m}_{ie}, \tag{14}$$

where $\dot{m}_{w-i}$ is the mass flow rate of component i induced by the thermochemical reaction, $\dot{m}_{iw}$ is the mass flow rate of component i caused by the chemical reaction and the overall diffusion of gas, and $\dot{m}_{ie}$ is the mass flow rate of component i in the gas from the outer edge of the boundary layer transition section to the ablation wall.

The heterogeneous ablation of C/SiC composites occurs under airflow (Fig. 9). On the composite surface, there appears a boundary layer with the ablation surface temperature (T_w), density (ρ_e), pressure (p_e), and airflow speed (u). All chemical, heat, and diffusive interactions were assumed to occur immediately on the interface $\sum$ of the composite and the boundary layer. Thus, all characteristics of gas do not change over the boundary layer thickness [32].

When the laser and airflow interact with the composite, the ablation of materials was characterized by the linear rate v, which motion along the normal to the ablation surface. In accordance with the models suggested in [33], the total rate v is a linear superposition of two constituents:

$$v = v_{TC} + v_{TM}, \tag{15}$$

v_{TC} is the summarized linear rate of the thermochemical ablation of composite under airflow, which consists of two parts, i.e., v_O and v_S. v_O is the linear rate of the chemical reaction of oxidizing, and v_S is the linear rate of sublimation of the chemical components of the composite.

$$v_{TC} = v_S + v_O, \tag{16}$$

v_{TM} is the summarized rate of the thermomechanical erosion of the composite, which consists of the erosion rates of the matrix (v_m) and the fiber (v_f).

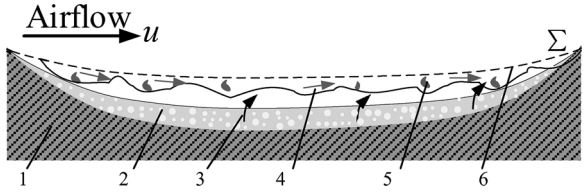

Fig. 9. Scheme of heterogeneous ablation of C/SiC composites under airflow: 1-initial composite, 2-pores in composite, 3- thermochemical ablation, 4-thermomechanical erosion. 5- ablation products. 6- boundary layer.

$$v_{TM} = v_m + v_f, \tag{17}$$

The ablation rate of sublimation of C/SiC can be described by [33]:

$$v_S = \frac{1}{\rho_w}\left(\alpha/c_p\right)\left(p_g^*/p_e\right)\exp\left(-\frac{E_{AS}M_S}{RT_w}\right), \tag{18}$$

where ρ_w is the density of the composite on the ablation surface, α/c_p is the heat transfer coefficient in a boundary layer, p_e is the local pressure of airflow, p_g^* is the constant pressure, M_S is the molecular mass of the sublimation reaction, E_{AS} the activation energy of the sublimation reaction, and R is the ideal gas constant. The ablation rate was inversely proportional to the local pressure of airflow (p_e). Thus, a low local pressure can increase the sublimation rate.

The ablation rate of the oxidation of C/SiC can be described by the Arrhenius equation:

$$v_O = \frac{1}{\rho_w}\sum\frac{M_i}{M_{O_2}}p_{O_2w}^n A_i\left(\frac{T_w}{T_0}\right)^m \exp(-\frac{E_{Ai}M_{iO}}{RT_w}), \tag{19}$$

where for the ith component: M_i is the molecular mass, M_{O2} is the relative molecular mass of oxygen, P_{O2w} is the oxygen partial pressure near the ablation surface, n is the reaction order, E_{Ai} and A_i is the activation energy and pre-exponential multiplier of the oxidation action, M_{iO} is the molecular mass of the oxidation reaction, and $(T_w/T_0)^m$ is the temperature correction coefficient.

The ablation rate of the erosion of fiber and matrix can be described by [32]:

$$v_{f\perp} = \frac{1}{\rho_f}\left(\frac{J_f^0 k_f}{c_f}\right)^{1/2}\left(\frac{6p_\sum}{\sigma_{f\perp}}\right)^{1/3}\left(\frac{RT_w}{E_{Af}}\right)^{1/2}\exp\left(-\frac{E_{Af}}{RT_w}\right), v_{f\parallel} = v_{f\perp}\left(\frac{\sigma_{f\perp}}{\sigma_{f\parallel}}\right)^{1/2}, \tag{20}$$

$$v_m = \frac{1}{\rho_m}\left(\frac{J_m^0 k_m}{c_m}\right)^{1/2}\left(\frac{6p_\sum}{\sigma_{mT}}\right)^{1/3}\left(\frac{RT_w}{E_{Am}}\right)^{1/2}\exp\left(-\frac{E_{Am}}{2RT_w}\right), \tag{21}$$

where $v_{f\perp}$ and $v_{f\parallel}$ are the rates of the external thermomechanical erosion of fibers in transverse and longitudinal directions; k_f, ρ_f, c_f and k_m, ρ_m, c_m are the heat-physical characteristics of the fibers and matrix, respectively; $p_\sum$ is the pressure head of airflow on the ablation surface; σ_{mT} is the ultimate strength of matrix in tension; $\sigma_{f\parallel}$ and $\sigma_{f\perp}$are the strength of fibers in longitudinal and perpendicular directions; J_f^0, E_{Af} and J_m^0, E_{Am} are pre-exponential multiplier and activation energy of thermal decomposition process. Meanwhile, $\rho_e\ u^2$ can be regarded as the contribution of airflow to the erosion effect:

$$p_\Sigma = \rho_e u^2, \tag{22}$$

The erosion effect is proportional to the kinetic energy of the airflow.

For transversally isotropic composites, two different components exist about the ablation rate of erosion [33]:

$$v_m = v_{m1}(n_1^2 + n_2^2) + v_{m2}n_3^2, \tag{23}$$

$$v_f = v_{f\perp}(n_1^2 + n_2^2) + v_{f\parallel}n_3^2, \tag{24}$$

where n_i is the component of normal vector $\mathbf{n}$, v_{m1} is the rate of the surface orthogonal to the axis n_3 (in-plane direction), and v_{m2} is the rate of the surface orthogonal to the axes n_1 and n_2 (thickness direction).

Some constants and parameters are given from [32,33]. Under the hypersonic air conditions, the ablation rate of sublimation increased due to decreased local pressure p_e, and the erosion rate also increased as a result of the significant increase in pressure head $p_\sum$. Therefore, the total ablation rate was greatly augmented in the hypersonic environment. The region downstream of the airflow in the ablation pit (M6.0, p_e = 2.55 kPa, $p_\sum$ = 175 kPa), which was substantially affected by the high-speed airflow in our study, was selected. The assumed

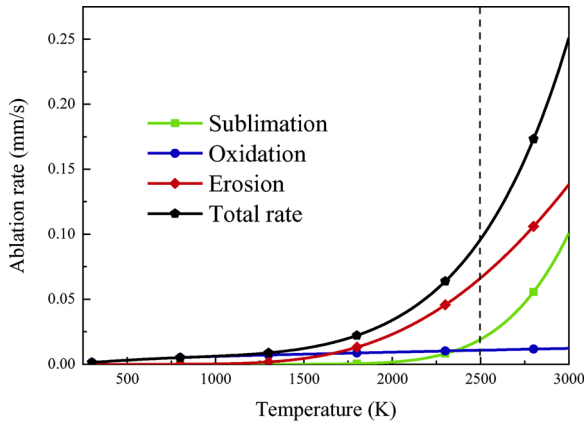

Fig. 10. The contribution of different mechanisms in ablation process under hypersonic airflow.

temperatures of the same region at different ablation times were 2500 and 3000 K. The contribution of different ablation mechanisms is shown in Fig. 10. The ablation rate of sublimation and erosion accounted for 19.88 % and 68.96 %, respectively, of the total rate at 2500 K; and 40.13 % and 55.03 %, respectively, of the total rate at 3000 K. The calculation values indicated that the mechanical erosion played a leading role in the ablation process of this region under a hypersonic airflow. The discussion only described the relationship of several ablation mechanisms semi-quantitatively. The strict quantitative calibration needs the systemic 3D coupled fluid–thermal–mechanical numerical model incorporated with detailed ablation models, which will be the focus of further work.

4. Conclusion

The laser ablation behavior of C/SiC composites was investigated in a hypersonic wind tunnel. Ablation morphologies, microstructure, ablation depth, and ablation rates were obtained and compared with those in the static air environment. Owing to hypersonic airflow, the convective heat on the ablation surface increased, and the deposition of ablation products decreased. The strong aerodynamic erosion effect resulted in altered macroscopic morphologies, increased ablation depth and width, and enhanced mass ablation rates (R_m) by 4–9 times.

The needle-like microstructure of carbon fibers exhibited rough and tattered morphologies at the center region, due to the impact by high-speed airflow and solid ablation products. SiC particles were blown away, and residual fibers and partially oxidized matrix remained at the transition region. Silicon oxides were deposited downstream of the airflow and had been massively exfoliated at the ablation edge region. Therefore, the oxidation reaction was aggravated. Ablation morphologies were also significantly different at the micro-scale, and the intense effects of aerodynamic erosion were both reflected macroscopically and microscopically. The effects of the laser ablation of the C/SiC composites subjected to the hypersonic airflow were the combination of sublimation, increased oxidation, aerodynamic cooling, and intense mechanical erosion. Finally, the ablation rate models of thermochemical ablations and thermomechanical ablation were introduced into the hypersonic airflow condition, and the contribution of different ablation mechanisms was evaluated semi-quantitatively.

CRediT authorship contribution statement

Zhe Wang: Investigation, Methodology, Writing - original draft. **Jiangtao Wang:** Investigation, Methodology. **Hongwei Song:** Conceptualization, Supervision, Writing - review & editing. **Wu Yuan:** Investigation. **Yuwen Liu:** Resources. **Te Ma:** Investigation. **Chenguang Huang:** Conceptualization.

Declaration of Competing Interest

The authors declare no conflict of interest.

Acknowledgements

Financial supports from the National Natural Science Foundation of China (Grant Nos. 91016025, 11472276, 11332011, 11972035, 11902322 and 11972033), and Strategic Priority Research Program of the Chinese Academy of Sciences (Grant No. XDA22000000), are gratefully acknowledged. The authors would also like to thank Professor Xiaowei Yin (Northwestern Polytechnical University) for the preparation of materials.

References

[1] R.R. Naslain, SiC-matrix composites: nonbrittle ceramics for thermo-structural application, Int. J. Appl. Ceram. Technol. 2 (2010) 75–84.
[2] M. Imuta, J. Gotoh, Development of high temperature materials including CMCs for space application, Key Eng. Mater. 164-165 (1999) 439–444.
[3] D. Glass, Ceramic matrix composite (CMC) thermal protection systems (TPS) and Hot structures for hypersonic vehicles, Aiaa International Space Planes & Hypersonic Systems & Technologies Conference (2008).
[4] R.E. Tressler, Recent developments in fibers and interphases for high temperature ceramic matrix composites, Compos. Part A Appl. Sci. Manuf. 30 (1999) 429–437.
[5] S. Schmidt, S. Beyer, H. Knabe, H. Immich, R. Meistring, A. Gessler, Advanced ceramic matrix composite materials for current and future propulsion technology applications, Acta Astronaut. 55 (2004) 409–420.
[6] L.T. Zhang, L.F. Cheng, X.G. Luan, H. Mei, Y.D. Xu, Environmental performance testing system for thermostructure materials applied in aeroengines, Key Eng. Mater. 313 (2006), 183-180.
[7] T. Cheng, W. Li, L. Wei, Y. Shi, Heat transfer and failure mode analyses of ultrahigh-temperature ceramic thermal protection system of hypersonic vehicles, Math. Probl. Eng. 2014 (2014) 1–11 (2014-7-1), 2014.
[8] D.M. Van Wie, D.G. Drewry, D.E. King, C.M. Hudson, The hypersonic environment: required operating conditions and design challenges: special section: ultra-high temperature ceramics (guest editors: joan Fuller and Michael D. Sacks), J. Mater. Sci. 39 (2004) 5915–5924.
[9] W. Yang, Z. Chen, S.J. Yu, Ablation behavior and mechanism analysis of C/SiC composites, J. Mater. Res. Technol. 5 (2016) 170–182.
[10] H. Li, L. Zhang, L. Cheng, Y. Wang, Ablation resistance of different coating structures for C/ZrB_2–SiC composites under oxyacetylene torch flame, Int. J. Appl. Ceram. Technol. 6 (2010) 145–150.
[11] Y. Bo, Z. Chen, J. Zhu, J. Zhang, J. Yun, Effects of ablation at different regions in three-dimensional orthogonal C/SiC composites ablated by oxyacetylene torch at 1800 °C, J. Mater. Process. Technol. 209 (2009) 3438–3443.
[12] C. Liu, L. Cao, J. Chen, L. Xue, X. Tang, Q. Huang, Microstructure and ablation behavior of SiC coated C/C–SiC–ZrC composites prepared by a hybrid infiltration process, Carbon 65 (2013) 196–205.
[13] D. Fang, Z. Chen, Y. Song, Z. Sun, Morphology and microstructure of 2.5 dimension C/SiC composites ablated by oxyacetylene torch, Ceram. Int. 35 (2009) 1249–1253.
[14] Z. Chen, D. Fang, Y. Miao, B. Yan, Comparison of morphology and microstructure of ablation centre of C/SiC composites by oxy-acetylene torch at 2900 and 3550°C, Corros. Sci. 50 (2008) 3378–3381.
[15] Y. Tang, M. Yue, X. Fang, X. Feng, Evolution of surface droplets and flow patterns on C/SiC during thermal ablation, J. Eur. Ceram. Soc. 39 (2019) 3566–3574.
[16] L. Luo, Y. Wang, L. Liu, L. Duan, G. Wang, Y. Lu, Ablation behavior of C/SiC composites in plasma wind tunnel, Carbon 103 (2016) 73–83.
[17] F. Monteverde, R. Savino, M.D.S. Fumo, A. Di Maso, Plasma wind tunnel testing of ultra-high temperature ZrB_2–SiC composites under hypersonic re-entry conditions, J. Eur. Ceram. Soc. 30 (2010) 2313–2321.
[18] J. Lachaud, Y. Aspa, G.L. Vignoles, Analytical modeling of the steady state ablation of a 3D C/C composite, Int. J. Heat Mass Transf. 51 (2008) 2614–2627.
[19] J.C. Han, X.D. He, S.Y. Du, Oxidation and ablation of 3D carbon-carbon composite at up to 3000 °C, Carbon 33 (1995) 473–478.
[20] J. Lachaud, Y. Aspa, Gr.L. Vignoles, Analytical modeling of the transient ablation of a 3D C/C composite, Int. J. Heat Mass Transf. 115 (2017) 1150–1165.
[21] G.L. Vignoles, Y. Aspa, M. Quintard, Modelling of carbon–carbon composite ablation in rocket nozzles, Compos. Sci. Technol. 70 (2010) 1303–1311.
[22] Q. Liu, L. Zhang, F. Jiang, L. Jia, L. Cheng, L. Hui, Y. Wang, Laser ablation behaviors of SiC–ZrC coated carbon/carbon composites, Surf. Coat. Technol. 205 (2011) 4299–4303.
[23] L. Long, Y. Huang, J. Zhang, Experimental investigation and numerical simulation on continuous wave laser ablation of multilayer carbon fiber composite, Proc. Inst. Mech. Eng. Part L J. Mater. Des. Appl. 231 (2015).
[24] P. Nan, Z. Shen, B. Han, X. Ni, The influences of laminated structure on the ablation characteristics of carbon fiber composites under CW laser irradiation, Opt. Laser Technol. 116 (2019) 224–231.
[25] Y. Tong, S. Bai, H. Zhang, Y. Ye, Laser ablation behavior and mechanism of C/SiC composite, Ceram. Int. 39 (2013) 6813–6820.

[26] X. Dang, X. Yin, X. Fan, Y. Ma, J. Wang, P. Ju, H. Song, Microstructural evolution of carbon fiber reinforced SiC-based matrix composites during laser ablation process, J. Mater. Sci. Technol. 35 (2019) 2919–2925.
[27] J. Wang, Y. Ma, Y. Liu, W. Yuan, H. Song, C. Huang, X. Yin, Experimental investigation on laser ablation of C/SiC composites subjected to supersonic airflow, Opt. Laser Technol. 113 (2019) 399–406.
[28] Y. Xu, S. Ren, W. Zhang, Thermal conductivities of plain woven C/SiC composite: micromechanical model considering PyC interphase thermal conductance and manufacture-induced voids, Compos. Struct. 193 (2018) 212–223.
[29] Y. Ma, X. Yin, X. Fan, P. Ju, X. Dang, Modification and toughening of 3D needled C/SiC composite by deformable MAX phase-based matrix, Mater. Sci. Eng. A 712 (2018) 397–405.
[30] X. Fan, X. Yin, L. Wang, L. Cheng, L. Zhang, Processing, microstructure and ablation behavior of C/SiC–Ti_3SiC_2 composites fabricated by liquid silicon infiltration, Corros. Sci. 74 (2013) 98–105.
[31] X. Chang, L. Chen, H. Gu, Y. Gang, Progress in studies on test facility and experimental technique for model SCRAMJET, Adv. Mech. (2003).
[32] Y.I. Dimitrienko, I.D. Dimitrienko, Effect of thermomechanical erosion on heterogeneous combustion of composite materials in high-speed flows, Combust. Flame 122 (2000) 211–226.
[33] Y.I. Dimitrienko, Thermomechanics of Composite Structures under High Temperatures, Springer, Netherlands, 2016.